Impact of coastal marsh eco-geomorphologic change on the prediction of saltwater intrusion under future sea level rise

Yu Zhang[1], Daniil Svyatsky[2], Joel C. Rowland[1], J. David Moulton[2], Zhendong Cao[2], Phillip J. Wolfram[3], Chonggang Xu[1], and Donatella Pasqualini[4]

[1]Earth and Environmental Sciences Division, Los Alamos National Laboratory, Los Alamos, NM, USA.

[2]Theoretical Division, Los Alamos National Laboratory, Los Alamos, NM, USA.

[3]Advanced Engineering Analysis, Los Alamos National Laboratory, Los Alamos, NM, USA.

[4]Analytics, Intelligence & Technology Division, Los Alamos National Laboratory, Los Alamos, NM, USA.

Corresponding author: Yu Zhang (yuzhang@lanl.gov)

Key Points:

- The effect of coastal marsh evolution on future saltwater intrusion is examined for the first time
- Marsh accretion under sea level rise may significantly reduce surface seawater inflow and prolong the surface seawater residence time
- Future saltwater intrusion on the evolved marsh landscape may become more sensitive to upland groundwater inflows

Abstract

Coastal saltwater intrusion (SWI) is one key factor that affects the hydrology, nutrient transport, and biogeochemistry of coastal marsh landscapes. Future climate change, especially intensified sea level rise (SLR), is expected to trigger SWI to encroach coastal freshwater aquifers more intensively. Numerous studies have investigated decadal/century scale SWI under SLR by assuming a static coastal landscape topography. However, coastal marshes are highly dynamic systems in response to SLR, and the impact of coastal marsh evolution on SWI has received very little attention. Thus, this study investigated how coastal marsh evolution affects future SWI with a physically-based coastal hydro-eco-geomorphologic model, ATS (Advanced Terrestrial Simulator). Our synthetic modeling experiments showed that it is very likely that the marsh elevation increases with future SLR, and a depression zone is formed due to the different marsh accretion rates between the ocean boundary and the inland. We found that, compared to the cases without marsh evolution, the marsh accretion may significantly reduce the surface saltwater inflow at the ocean boundary, and the evolved topographic depression zone may prolong the residence time of surface ponding saltwater, which causes distinct subsurface salinity distributions. We also found that the marshland may become more sensitive to the upland groundwater table that controls the freshwater flux to the marshes, compared with the cases without marsh evolution. This study demonstrates the importance of marsh evolution to the freshwater-saltwater interaction under sea level rise and can help improve our predictive understanding of the vulnerability of the coastal freshwater system to sea level rise.

Keywords: Saltwater intrusion, Coastal marsh evolution, Sea level rise, Freshwater-saltwater interface, Groundwater table, Coastal aquifer vulnerability

1 Introduction

Coastal wetlands, unique landscapes that connect the terrestrial landscape and the ocean, are some of the most productive ecosystems on Earth (Tiner, 2013). Climate change, especially sea level rise (SLR) under a warming climate, is one of the biggest threats to the stability and sustainability of coastal wetland ecosystems (Burkett & Kusler, 2000). SLR-driven impacts on coastal marsh ecosystems are strongly affected by changes in coastal hydrology (Zhang et al., 2019). The rising sea level alters the balance of coastal freshwater-saltwater interaction both on coastal wetland surface and in the subsurface aquifer causing the changes in saltwater intrusion (SWI), thereby affecting soil water salinity (Guimond & Tamborski, 2021; Sorensen et al., 1984; Sousa et al., 2010), triggering the mortality of salt-intolerant vegetation (Silvestri & Marani, 2004), and eventually altering the ecosystem functions of coastal wetlands (Burkett & Kusler, 2000). Therefore, investigating the response of SWI to SLR is critical for our understanding of the SLR impact on coastal wetland ecosystems.

Numerous studies have attempted to predict and/or assess the impact of SLR on SWI for decades. These studies have aimed to track the movement of the freshwater and saltwater interface in coastal aquifers driven by SLR at global (e.g., Ferguson & Gleeson, 2012; Michael et al., 2013), regional (e.g., Oude Essink et al., 2010; Zhang et al., 2018, 2019), and local/transect scales (e.g., Ataie-Ashtiani et al., 2013; Carretero et al., 2013; Chang et al., 2011; Chen et al., 2015; Giambastiani et al., 2007; Hughes et al., 2009; Ketabchi et al., 2014, 2016; Langevin & Zygnerski, 2013; Loáiciga et al., 2012; Lu et al., 2015; Masterson & Garabedian, 2007; Mazi et al., 2013; Morgan et al., 2013; Payne, 2010; Rasmussen et al., 2013; Sefelnasr & Sherif, 2014; Sorensen et al., 1984; Vandenbohede et al., 2008; Vu et al., 2018; Watson et al., 2010; Werner et al., 2012; Werner & Simmons, 2009; Yang et al., 2015). By using analytical or numerical

models, these studies examined SWI in coastal aquifers under SLR, especially under the influence of different environmental settings, such as regional-scale hydrologic connectivity, upland groundwater boundary condition, land surface inundation, groundwater extraction, and recharge. For example, *Zhang et al.* (2018, 2019) investigated the groundwater flow path and SWI of the coastal wetlands in North Carolina, USA, by considering regional-scale coastal hydrologic connectivity. They found that aquifers with the largest seasonal changes of SWI are located hundreds of meters away from the shoreline, where freshwater strongly interacts with saltwater. In terms of the effect of upland boundary conditions on SWI, *Werner and Simmons* (2009) and *Werner et al.* (2012) found that SLR impact is more extensive in unconfined aquifers with a head-controlled inland boundary, compared with confined aquifers. *Carretero et al.* (2013) found that SWI increased linearly with SLR in aquifers with a flux-controlled boundary condition, but increased nonlinearly with a head-controlled boundary condition. In terms of the effect of groundwater extraction and freshwater supply (recharge), *Loáiciga et al.* (2012) found that groundwater extraction was the predominant driver of SWI in one coastal aquifer in Monterey, California, compared with the effect of SLR. Using the coastal aquifer at the Western Baltic Sea as an example , *Rasmussen et al.* (2013) found that the SWI in flux-controlled aquifers is more sensitive to recharge than SLR. Likewise, *Ataie-Ashtiani et al.* (2013) found that surface inundation may induce significantly more extensive SWI than SLR. Each of these studies provided insights into understanding SWI under SLR in the temporal scales of decades and centuries, however, none of them considered the effect of coastal landscape topographic change, which may have a significant impact on SWI by altering flow paths and residence time.

The evolution of coastal marsh landscape topography under SLR has been explored extensively by the coastal geomorphologic community. Many studies have predicted coastal

marsh evolution as a function of sediment erosion and deposition and found that coastal marshes are not static but dynamic landscapes. Coastal marshes are very likely to keep pace with the rates of SLR at decadal to century scales due to the net sedimentation on the marshlands (e.g., Best et al., 2018; D'Alpaos et al., 2007; Kirwan, Temmerman, et al., 2016; Kirwan, Walters, et al., 2016; Kirwan & Murray, 2007; Kirwan & Temmerman, 2009; Mariotti & Fagherazzi, 2010; Zhang et al., 2020). With the changes in marsh geomorphology, the topographic and hydraulic gradient among the land, river, and ocean will change, which will alter the seawater flow path and storage (Winn et al., 2006). However, so far, there is a critical knowledge gap on how the evolution of coastal landscape may affect the SWI under SLR. This could severely limit our capability to estimate the vulnerability of coastal aquifer to SWI under SLR. To fill this knowledge gap, in this study, we used synthetic coastal marsh transects to examine the effect of coastal marsh evolution on coastal SWI under SLR. We simulated coastal marsh evolution and SWI on the coastal marsh transects under different rates of SLR over 100 years by using a coastal marsh evolution model and a density-dependent solute transport model in the Advanced Terrestrial Simulator (ATS) (Coon et al., 2016). We evaluated the impacts of coastal marsh evolution on SWI by comparing the surface and subsurface hydrologic characteristics between the SWI simulations with and without considering coastal marsh evolution. The surface hydrologic characteristics include seawater propagation, inflow, surface salt concentration, and surface seawater penetration. The subsurface hydrologic characteristics include subsurface water salinity distribution, seawater inflow, and the displacement of the freshwater-saltwater interaction. We hypothesized that coastal marsh evolution cannot be ignored when evaluating coastal SWI under SLR at a decadal or century scale because marsh evolution may significantly affect the surface seawater inflow rate and the surface water residence time, therefore change

SWI. The insights gained from this study can help improve our understanding of the vulnerability of coastal freshwater systems to SWI.

In this paper. we first introduce the numerical model, experiment and scenario designs, and evaluation metrics in Section 2, after which we present and analyze the results from the numerical experiments for marsh evolution and SWI in Section 3. Lastly, Section 4 discusses the implication of this study for understanding SWI under SLR from a coupled hydro-eco-geomorphologic framework, its representativeness, uncertainties, and outlined future work, followed by conclusions in Section 5.

2 Materials and Methods

2.1 Mathematical models

This study used the Advanced Terrestrial Simulator (ATS) (Coon et al., 2016) to simulate SWI and coastal marsh evolution under SLR conditions. ATS is a multi-process high-performance computing simulator with process kernels (PKs) for surface and subsurface hydrology, energy balance, thermal dynamics, sediment transport, solute transport, coastal marsh evolution, and marsh vegetation dynamics. Here we used some ATS PKs to configure a saltwater intrusion model and a coastal marsh evolution model.

2.1.1 The configuration of coastal saltwater intrusion in ATS

We used the SWI configuration in ATS (hereinafter referred to as SWI model) to simulate the salinity change of surface and subsurface water by coupling surface and subsurface hydrologic processes with density-dependent solute transport processes. The integrated hydrologic processes include a two-dimensional (2-D) diffusive-wave approximation of surface flows (Vreugdenhil, 1994) and a variably saturated three-dimensional (3-D) Richards equation

(Richards, 1931) for subsurface flows. The governing system of PDEs for surface and subsurface fluid mass balance is as follows,

$$\begin{cases} \frac{\partial d\rho_1}{\partial t} = -\nabla_1(\rho_1 d\mathrm{u}) - I_w \\ \frac{\partial \theta\sigma\rho_2}{\partial t} = -\nabla_2(\rho_2 q) + I_w \end{cases} \quad (1)$$

where $\rho_1(C_1)$ and $\rho_2(C_2)$ are the surface and subsurface fluid density (kg/m^3) which are functions of surface and subsurface salt concentrations (dimensionless), C_1 and C_2, respectively; d is the surface water depth (m); θ is the subsurface water content; σ is the soil porosity; u is the depth-averaged surface flow velocity (m/s) which is, according to the diffusive wave approximation, defined as follows:

$$\mathrm{u} = -\frac{d^{\frac{2}{3}}}{n(|\nabla(z+d)|)^{\frac{1}{2}}}\nabla(z+d) \quad (2)$$

where z is surface elevation (m); n is the Manning's coefficient of roughness ($s/m^{1/3}$); q in Eq. 1 is the subsurface water flow velocity (m/s) defined by Darcy law:

$$q = -\frac{k_r K}{\mu}\nabla h \quad (3)$$

where k_r and K are a relative (dimensionless) and absolute permeabilities (m^2), respectively, μ is fluid dynamic viscosity (kg/m/s) and h is subsurface hydraulic head (m). I_w is the mass source/sink term (kg/s m^2) representing the infiltration or exfiltration (positive in the downward direction)

In Eq. 1, the density is a linear function of water concentration (Simmons et al., 2001):

$$\rho = \rho_0 + a(C - C_0), \quad (4)$$

where ρ is the fluid density for surface water or subsurface water (kg/m^3); C is the fluid salt concentration for surface and subsurface water (dimensionless); ρ_0 is the fluid density at a base concentration, C_0; a is a constant coefficient of density variability.

The generic form of saltwater concentration is calculated based on the salt mass balance equation following *Herbert et al.* (1988) and *Simmons et al.* (2001)

$$\begin{cases} \frac{\partial(d\rho_1 C_1)}{\partial t} = -\nabla_1(d\rho_1 u C_1) + \nabla_1[d\rho_1(D_0 + D)\cdot\nabla_1 C_1] - \mathrm{I_{salt}} \\ \frac{\partial(\theta\sigma\rho_2 C_2)}{\partial t} = -\nabla_2(\theta\sigma\rho_2 q C_2) + \nabla_2[\theta\sigma\rho_2(D_0 + D)\cdot\nabla_2 C_2] + \mathrm{I_{salt}} \end{cases} \quad (5)$$

where C_1 and C_2 are the salt concentration of surface and subsurface water (dimensionless), respectively. D_0 is the molecular diffusivity (m^2/s). $\boldsymbol{D}$ is the transverse and longitudinal dispersivities; Likewise, $\mathrm{I_{salt}}$ is the mass source/sink term (kg/s m^2) representing the infiltration or exfiltration (positive in the downward direction). The capability of the SWI model in capturing saltwater intrusion through surface and subsurface flow under tidal conditions was well validated by comparing the model simulation with a lab experiment of SWI with tidal variation by *Kuan et al.* (2019) (see the validation results in the supplementary information Text S1 and Figs. S1 and S2).

2.1.2 The configuration of coastal marsh evolution in ATS

For the marsh evolution modeling, we used the coastal marsh evolution model (hereinafter referred to as Sed model) configured by the 2-D surface flow, sediment transport and marsh evolution PKs in ATS. The Sed model tracks the change of marsh surface elevation as a function of sediment erosion, sediment settling, sediment trapping by vegetation, and vegetation organic matter production. Namely,

$$\frac{dz}{dt} = \frac{1}{1-\sigma}\left(D_s + D_t + D_{org} - E\right) \quad (6)$$

where z is the surface elevation (m); t is the time (s); σ is the porosity of bed sediment; D_s is the inorganic sediment settling rate (m/s); D_t is the inorganic sediment trapping rate due to the effect of vegetation canopy (m/s); D_{org} is the organic matter production rate (m/s); E represents local sediment erosion rate (m/s).

The Sed model follows the forms of sediment erosion and deposition in D'Alpaos et al. (2007), but improved the representation of surface hydrodynamics, instead of using an equilibrium assumption for surface hydrodynamics. Specifically, in the Sed model, the surface hydrodynamics due to tide and SLR is represented by a depth-averaged diffusive-wave scheme (Eq. 2) considering the spatial and temporal variations of water propagation landward. Sediment erosion (E in Eq. 6) is estimated as a linear function of dynamic bed shear stress depending on surface water flow velocity. Erosion occurs when the bed shear stress (τ_0) due to water flow is greater than the critical shear stress (τ_e) for erosion. Namely,

$$E = \begin{cases} \alpha\left(\frac{\tau_0}{\tau_e} - 1\right) & if\ \tau_0 > \tau_e \\ 0 & if\ \tau_0 < \tau_e \end{cases}, \quad (7)$$

where α is the erosion coefficient. Likewise, sediment settling (D_s in Eq. 6) describes the process that particulates settle to the bottom of a liquid and form sediment due to gravity, which is also assumed as a linear function of dynamic bed shear stress. Sediment settling occurs when the bed shear stress (τ_0) is smaller than the critical shear stress (τ_d) for settling, viz

$$D_s = \begin{cases} w_s C\left(1 - \frac{\tau_0}{\tau_d}\right) & if\ \tau_0 < \tau_d \\ 0 & if\ \tau_0 > \tau_d \end{cases}. \quad (8)$$

where w_s is the settling velocity (m/s); C is the suspended sediment concentration (dimensionless). Sediment trapping by vegetation (D_t in Eq. 6) is given by

$$D_t = CU\epsilon d_s n_s \min[h_s, h_w] \tag{9}$$

where D_t is a function of water flow velocity (U), a capture efficiency of vegetation stems (ϵ), water depth (h_w), and several vegetation characteristics, such as plant stem diameter (d_s), stem density (n_s), and vegetation height (h_s). The vegetation properties are determined by vegetation biomass, which is assumed as a linear function of marsh surface elevation relative to the mean highest tide level. Also, the vegetation organic matter production (D_{org} in Eq. 6) is a linear function of vegetation biomass, viz

$$D_o = K_b \frac{B}{B_{max}}, \tag{10}$$

where K_b is the maximum production rate of belowground organic material [m/s]; B is the aboveground plant dry biomass at the current time [g/m^2]; and B_{max} is the maximum vegetation biomass [g/m^2]. In this study, we assume that the aboveground biomass of the salt-tolerant marsh vegetation linearly increases with the inundation level (Morris et al., 2002). The details of the questions are referred to D'Alpaos et al. (2007) and Zhang et al. (2020).

An offline coupling approach was used in this study to integrate the Sed model and the SWI model (an online coupling scheme is under development). Specifically, we 1) first simulate the coastal marsh evolution by using the Sed model and 2) use the simulated future surface elevation from step (1) as the initial topographic and morphologic condition to simulate future SWI until equilibrium by using the SWI model.

211 2.2 Numerical experiment design

212 To investigate the effect of marsh evolution on SWI, we designed two 2-D synthetic
213 coastal marsh transects that include a 1 m wide coastal marshland (2000 m long) and upland
214 region (1000 m long) with different slopes to represent real coastal marshes at the Atlantic coast,
215 particularly the Delaware Bay and Chesapeake Bay areas (see Fig. 1). We assumed that the
216 coastal marshland is covered by salt-tolerant marsh species, such as *Spartina (Morris et al.,*
217 *2002)*. The slope of the coastal marsh (1:2500) represents an averaged slope of the coastal marsh
218 transects in Delaware Bay, USA, measured by this study. The upland slopes of 1:1000 and 1:250
219 in this area are used to represent different upland controls on surface-subsurface water
220 propagation and sediment transport (Fagherazzi et al., 2019). We assumed a homogeneous
221 landscape with homogeneous surface roughness and homogeneous soil properties, such as
222 surface Manning's coefficient, soil porosity, soil hydraulic conductivity, and van Genuchten
223 water retention parameters (see the details of parameter values in Table 1). The soil thickness at
224 the upland and the ocean boundaries are 20 m and 18.2 m, respectively, based on the
225 measurements in *Sanford et al.* (2012).

226 The hydrodynamics are driven by tides and SLR at the ocean boundary. Initially, the
227 mean sea level (MSL) is equal to 0 m, the elevation of the current coastal marsh near the ocean
228 boundary (see Fig. 1). We adopted two widely-used future global mean SLR scenarios based on
229 the Representative Concentration Pathways (RCP) 4.5 and RCP 8.5 scenarios in Phase 5 of the
230 Coupled Model Intercomparison Project (CMIP5) (Spencer et al., 2016) for our numerical
231 experiments, including (1) a relatively low SLR rate of 0.5 m/100-yr (Da Lio et al., 2013; Ganju
232 et al., 2020; Kirwan & Temmerman, 2009; Sefelnasr & Sherif, 2014; Spencer et al., 2016) and
233 (2) a relatively high SLR rate of 1 m/100-yr (Carretero et al., 2013; Langevin & Zygnerski,

2013; Lu et al., 2015; Michael et al., 2013; Sefelnasr & Sherif, 2014; Watson et al., 2010; Yang et al., 2015). We applied a sinusoidal semi-diurnal tide with a tidal range of 1.6 m based on the National Oceanic and Atmospheric Administration (NOAA) tide and current observation at the Delaware Bay, USA (Cape May Station, station ID: 8536110).

Freshwater supply in the coastal aquifer is controlled by the hydrostatic groundwater table (GWT) at the upland boundary (the left boundary of the domain in Fig. 1). This study used three upland GWT scenarios to represent (1) a present-day upland GWT condition (1.3 m above the initial MSL), (2) a future GWT condition with increased groundwater extraction and/or a drier climate (0.9 m above the initial MSL), and (3) a future GWT condition with a wetter climate (1.8 m above the initial MSL), respectively. To simplify the control factors and present a more focused study on the effect of marsh evolution on SWI, we did not include the effect of rainfall recharge in this study, which will be explored in future work. We used a head-controlled upland GWT boundary condition, which may predict more SWI than the flux-controlled upland boundary condition for unconfined aquifers (Werner & Simmons, 2009). Therefore, our scenarios may represent a relatively more aggressive prediction of SWI under SLR. All scenarios are summarized in Table 2.

The 2-D model domain in Fig. 1 was decomposed into logically structured mesh with a horizontal resolution of ~5 m and vertical resolution of ~1 m (20 layers). We simulated 100-yr marsh evolution, and the SWI experiments were simulated until the freshwater-saltwater interface reached an equilibrium state.

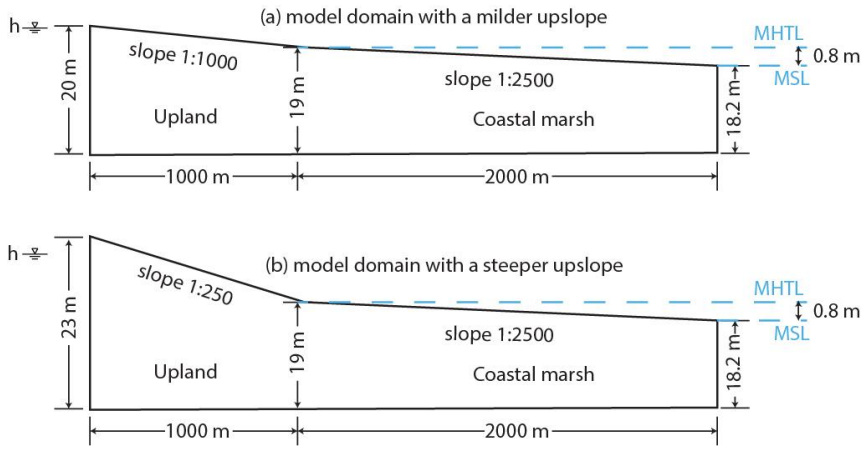

Figure 1. Sketches of the 2-D model domain. The surface elevation at the ocean boundary (right side) is 0 m. The elevation at the upland boundary is 1.8 m for the milder upslope domain and 4.8 m for the steeper upslope domain. MHTL stands for the mean highest tide level and MSL is mean sea level. The present-day MSL is at 0 m level. h at the left side of the domain indicates the upland groundwater level. Three upland groundwater level scenarios are used: h = 1.3 m (present-day level), h = 1.8 (reflecting future wetter climate), and h = 0.9 m (reflecting future drier climate or more groundwater extraction)

Table 1. Key parameter values used in the numerical experiments

	Parameters	Values	References
SWI-related parameters	Porosity	0.46	(Kuan et al., 2012)
	Hydraulic conductivity (m/day)	10	(Kuan et al., 2012)
	Manning's n (s $m^{-1/3}$)	0.06	(Arcement & Schneider, 1989)
	Diffusion coefficient (m^2 s^{-1})	1.00E-09	(Kuan et al., 2012)
	Longitudinal dispersivity coefficient (m)	0.002	(Kuan et al., 2019)
	Transversal dispersivity coefficient (m)	0.0004	(Kuan et al., 2019)
	van Genuchten α for water retention (m^{-1})	0.48	(Benson et al., 2014)
	van Genuchten n for water retention	2.54	(Benson et al., 2014)
	Residual saturation	0.1	(Kuan et al., 2012)
	Saltwater concentration in the ocean (kg salt per kg seawater)	0.0357	(Michael et al., 2013)
Marsh	Sediment concentration in the	50	(Kirwan, Walters, et al., 2016)

evolution-related parameters	ocean (mg/L)		
	Erosion coefficient ($\frac{kg}{m^2 s P_a}$)	1.12E-04	(D'Alpaos et al., 2007)
	Critical shear stress for erosion (P_a)	0.4	(Thompson et al., 2004)
	Critical shear stress for deposition (P_a)	0.1	(Parchure Trimbak M. & Mehta Ashish J., 1985)
	Sediment settling velocity ($\frac{m}{s}$)	1.00E-04	(Riazi & Türker, 2019)
	Belowground organic production ($\frac{m}{yr}$)	0.003	(Morris et al., 2016)

Table 2. The numerical experiment cases with different upland slope, SLR, and GWT scenarios

	Milder upland slope		Steeper upland slope	
	Higher SLR	Lower SLR	Higher SLR	Lower SLR
Medium upland GWT (h=1.3 m) (present-day scenario)	Case 1	Case 2	Case 3	Case 4
High upland GWT (h=1.8 m) (wetter climate scenario)	Case 5	Case 6	Case 7	Case 8
Low upland GWT (h=0.9 m) (drier climate and/or more groundwater extraction scenario)	Case 9	Case 10	Case 11	Case 12

2.3 Evaluating the effect of marsh evolution on SWI under SLR and tides

We evaluated the effect of marsh evolution on SWI by comparing the SWI simulation with and without marsh evolution. Specifically, we created two groups of experiments. Each group consisted of all 12 experimental cases listed in Table. 2. The first group of experiments was based on the current marsh topography as illustrated in Fig. 1. SWI was simulated under different rates of SLR and different levels of the upland GWT in the future 100 years without considering coastal marsh evolution. In contrast, the second group conducted the same SWI

simulations as the first group experiments but used the marsh topography from the marsh evolution simulations in the future 100 years as the topographic condition. We examined the surface and subsurface freshwater and saltwater changes in the two groups of numerical experiments. Specifically, we analyzed the changes in surface seawater propagation, inflow, concentration, and infiltration and subsurface water salinity, seawater inflow, and the displacement of the freshwater-seawater interface.

3 Results

3.1 Coastal marsh evolution driven by tidal and SLR forcing

With the SLR rates of 0. 5 m/100-yr and 1 m/100-yr, the future MSL increases to 0.5 m and 1 m in 100 years, respectively. Accordingly, the mean highest tide levels (MHTL, equal to MSL + tidal amplitude) rise from 0.8 m to 1.3 m and 1.8 m, respectively. Driven by the future SLR, our modeling results showed that the future marsh elevation rises substantially with SLR and with a larger increase near the ocean boundary and a smaller increase for the inland marsh (Figs. 2a and b) due to a gradient in sedimentation rates (Fig. 3). Therefore, a topographic depression forms in the middle of the marshland. The future elevations near the ocean boundary are close to the future MHTLs under both the higher and lower SLR rates. Correspondingly, the vegetation co-evolves with the topographic change and future inundation condition. The salt-tolerant vegetation biomass is modeled to increases with inundation level, which results in higher vegetation biomass in the middle of the domain and lower vegetation biomass at the ocean and upland sides (Figs. 2c and d). Relative to the initial marshland (the gray dashed lines in Figs. 2c and d from 1000m to 3000m from the upland boundary), there was a landward expansion of marsh vegetation that varied with SLR and upland slopes. For example, the marsh vegetation

294 covers the entire upland region in the case with the milder slope and higher SLR rate (the light
295 green line in Fig. 2c) because the future MHTL (1.8 m) is the same as the elevation of the upland
296 boundary leading to an inundation condition favorable for vegetation growth. For the cases with
297 the steeper upland slope, a large portion of the upland areas is still higher than the MHTL,
298 therefore no vegetation presents on the upland areas (Fig. 2d).

299 Among sedimentation rates across the domain, the sediment settling rate is the greatest
300 near the ocean boundary (the light blue lines in Fig. 3) because of a higher sediment
301 concentration near the ocean boundary. Moving landward, the sediment settling rate decreases
302 due to a lower sediment concentration, but the vegetation organic matter production rate
303 increases because of higher vegetation biomass, which contributes more to the sedimentation of
304 the inland marsh (the purple lines in Fig. 3). Vegetation sediment trapping is more significant
305 near the ocean boundary where the sediment concentration and flow velocity are higher. Moving
306 landward, due to the decrease of sediment concentration and flow velocity, the trapping effect
307 gradually vanishes (the orange lines in Fig. 3). Due to the vegetation effect on reducing water
308 flow velocity, sediment erosion is only observed at the beginning of the simulation when the
309 future SLR is applied to the domain boundary (not shown). Later in the simulation, the surface
310 elevation increases due to a higher sedimentation rate. Therefore, the seawater inflow velocity
311 decreases because of a decrease of the hydraulic gradient between the land and the ocean, and
312 the erosion rate drops to zero.

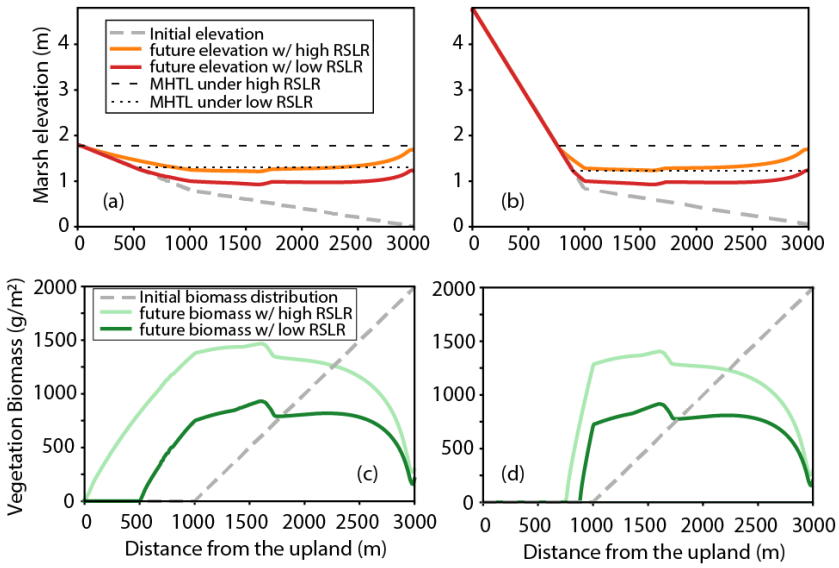

313

314 *Figure 2. The distribution of future elevation and vegetation biomass of the domain with a milder upland slope (a and c) and a*
315 *steeper upland slope (b and d). The gray dashed lines indicate the initial surface elevation and vegetation biomass distribution,*
316 *respectively. MHTL stands for the mean highest tide level. RSLR is the rate of sea level rise.*

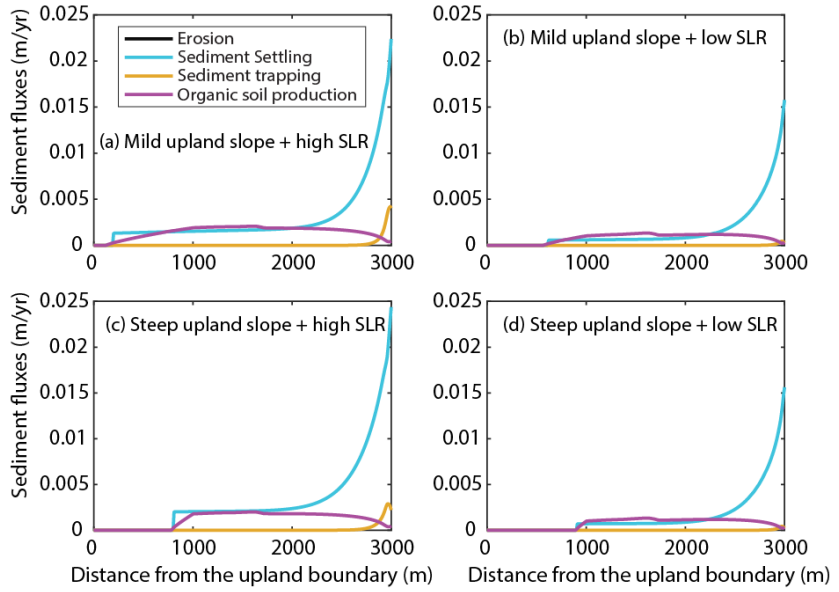

317

318 *Figure 3. The spatial distribution of the sediment fluxes at the end of the 100-year simulation. The plots with various colors*
319 *represent different fluxes in different scenarios.*

320 ## 3.2 SWI with and without marsh evolution

321 ### 3.2.1 The influence of marsh evolution on coastal hydrodynamics

322 After predicting the topographic change of the coastal marsh landscapes 100 years in the

323 future, we compared the SWI under SLR with and without considering the marsh evolution. For

both SLR rates, the upland GWT is held fixed at 1.3 m above the initial MSL (0 m), but the future MSL increases (see details of the MSL rise in Subsection 3.1). Without considering marsh topographic change in the future, the rising sea level increases the hydraulic gradient between the ocean and the marshland, thus more saltwater was predicted to flow onto the marshland with a relatively larger maximum inflow rate (~0.25 m^3/s) under the higher SLR scenario and a relatively lower rate (~0.16 m^3/s) under the lower SLR scenario (the gray bars in Fig. 4). However, considering marsh evolution, the marsh surface elevation increases with SLR, especially for marshland near the ocean boundary (e.g., Fig. 2a and b), which decreases the hydraulic gradient between the ocean and the marshland. Thus, the saltwater maximum inflows are predicted to be ~0.009 m^3/s for the higher SLR rate scenario and ~0.0048 m^3/s for the lower SLR rate scenario (the black bars in Fig. 4). These rates are two orders of magnitude smaller than the maximum inflow rates without considering marsh evolution.

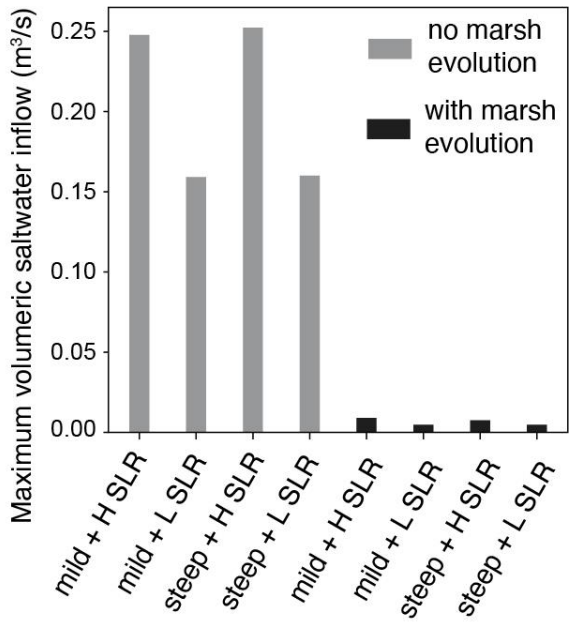

Figure 4. The maximum seawater inflows under future sea level for the simulations with and without considering coastal marsh evolution. The gray and black bars indicate the simulated seawater inflow without and with considering marsh evolution, respectively.

The marsh topographic change also affects surface seawater propagation, ponding water depth, surface water residence time, and saltwater concentration on the marsh surface. For example, Figure 5 shows the surface water propagation and saltwater concentration for the cases without considering marsh evolution (the top four plots with gray backgrounds) and with marsh evolution (the bottom four plots with white backgrounds). Without considering marsh evolution, seawater propagates landward during the high tides and causes a surface inundation with a maximum inundation depth higher than 1.3 m near the ocean boundary (the upper dashed lines in Fig. 5a, b, c, and d). During the high tides, the saltwater concentration in the ponding water is almost the same as the concentration in the ocean (3.5%; the blue dashed lines in Fig. 5a, b, c, and d), except for the upland regions, where the subsurface freshwater exfiltrates to the surface and dilutes the surface saltwater. During the low tides, the surface ponding water flows out from the marsh domain (the lower dashed lines in Fig. 5a, b, c, and d). Therefore, the residence time for surface saltwater is tightly controlled by the tidal frequency (~12 h).

In contrast, considering marsh evolution, the depression zone in the middle of the marshland significantly changes the surface water propagation. Saltwater flows onto the marshland during the high tides with a much smaller inflow rate as illustrated in Fig. 4, and then the saltwater gradually accumulates in the depression zone without flowing out from the domain during the low tides, which largely increases the residence time of saltwater (the black dashed lines in Fig. 5e, f, g, and h). A large portion of the surface ponded saltwater exits the marsh surface only through infiltration. Meanwhile, freshwater flows into the depression zone through subsurface freshwater exfiltration. In the cases with a higher SLR rate (Figs. 5e and g), the upland GWT (1.3 m) is lower than the future MHTL (1.8 m). For most of the time during a tidal cycle, fresh groundwater cannot easily flow into the marsh aquifer. Thus, at equilibrium, the

surface ponding water consists almost of saltwater with very little freshwater, and the surface saltwater concentration is almost equal to the concentration in the ocean for the entire surface ponding water (the blue lines in Figs. 5e and g). However, in the cases with a lower SLR rate (Figs. 5f and h), the upland GWT (1.3 m) is at the same level as the future MHTL (1.3 m). Fresh groundwater can be more easily flow into the marsh aquifer and exfiltrate to the surface when the instantaneous sea level is below the MHTL during a tidal cycle. Thus, a larger amount of fresh groundwater accumulates in the depression zone to dilute saltwater inflow. Therefore, we only observed an increase of surface saltwater concentration near the ocean boundary (the blue lines in Figs. 5f and h).

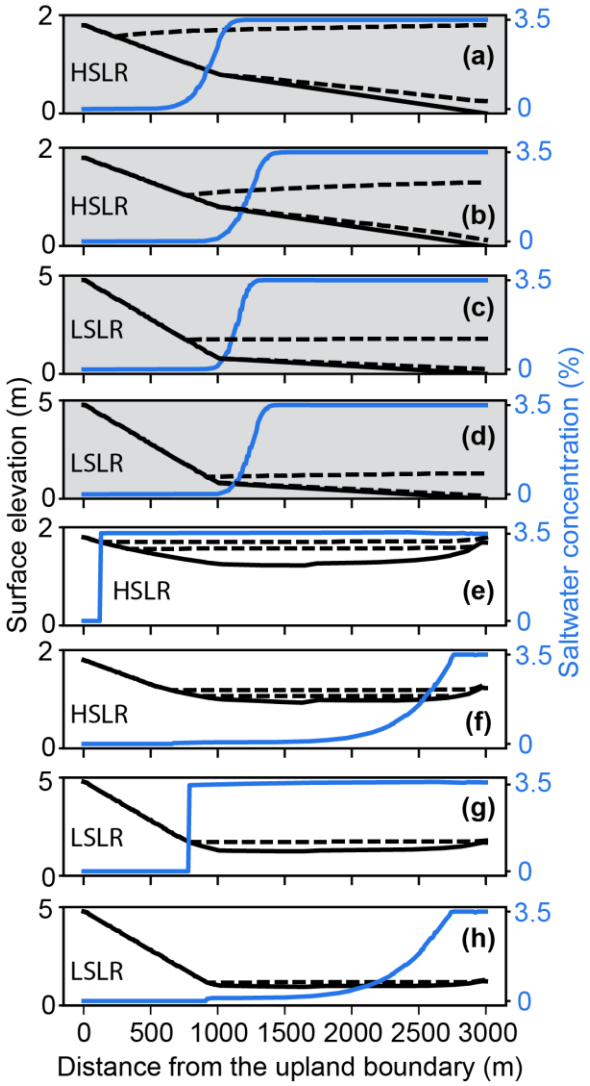

Figure 5. The surface water propagation and associated surface water concentration in the simulations with and without the considerations of marsh topographic change. (a), (b), (c), and (d) with the gray background are the cases without considering marsh evolution. (e), (f), (g), and (h)are the cases considering marsh evolution. The black solid lines are the surface elevation. The black dashed lines indicate the maximum and minimum surface water propagation under the high and low tides. The blue lines indicate the distribution of the saltwater concentration under the maximum surface water propagation conditions. HSLR and LSLR stand for the higher and lower SLR rate scenarios, respectively.

3.2.2 Subsurface salinity distribution

Under the present-day condition (upland GWT=1.3m) without SLR, Figs. 6a and b show the equilibrium salinity distribution in the aquifer with milder and steeper upland slopes, respectively. The toes and heads of the freshwater-saltwater interfaces (the interface between the blue and the cyan colors) are at ~1250 m and ~1500 m from the upland boundary, respectively.

Starting from this present-day equilibrium condition, we simulated the SWI under SLR. For the cases without considering marsh evolution (Figs. 6c, d, e, and f), we predicted an increase of SWI with the increase of SLR magnitudes. Both the toes and heads of the freshwater-saltwater interfaces are observed to move landward 500m to 1000m under the lower and higher SLR rates. The increases in SWI are attributed to the SLR-induced surface saltwater infiltration and subsurface lateral saltwater inflow. With the increased sea level, more surface seawater infiltrates to the subsurface aquifer. Meanwhile, more seawater flows into the aquifer directly through the subsurface lateral flow due to the increased hydraulic gradient between the sea level and the inland water table. We analyzed the changes in surface saltwater infiltration and subsurface lateral inflows from the beginning of the simulation to the end when the subsurface salinity distribution reached an equilibrium (see Fig. S3 and Text S2). In general, the surface saltwater infiltration had a much larger contribution to the subsurface SWI than the subsurface lateral inflow (see the blue solid lines in Fig. S3) due to the high inundation level during the high tides as illustrated in Fig. 5.

When marsh evolution was included, the depression zone formed by the marsh evolution process significantly increases surface water residence time. This occurs even though the simulated surface saltwater inflow and surface inundation depth at the ocean boundary (illustrated in Figs. 4 and 5) are much lower than the simulations without marsh evolution, Therefore, the surface ponding water accumulates seawater and prolongs the time of surface saltwater infiltration in contributing to the landward movement of the freshwater-saltwater interface. Thus, under the higher SLR rate, the equilibrium freshwater-saltwater interfaces almost reach the upland boundary (Figs. 6g and h), similar to the simulations without marsh evolution. However, under the lower SLR rate, more freshwater can flow into the domain due to a lower

hydraulic gradient between the sea level (0.5 m) and the upland GWT (1.3 m), there is no significant increase in saltwater concentration in the surface ponding water (e.g., the blue lines in Figs. 5f and h). Therefore, even though the surface saltwater infiltration still dominates the SWI (the blue dashed lines in Figs. 3Sb and d), its rate is smaller than the rate under the higher SLR rate and is located only near the ocean boundary (Figs. 5f and h). We see a distinct subsurface saltwater distribution at equilibrium under the lower SLR rate: the toe of the freshwater-saltwater interface moves towards the upland boundary, but the freshwater-saltwater interface near the marsh surface moves toward the ocean boundary. More freshwater occupies the upper part of the aquifer in the middle of the marshland (Figs. 5i and j).

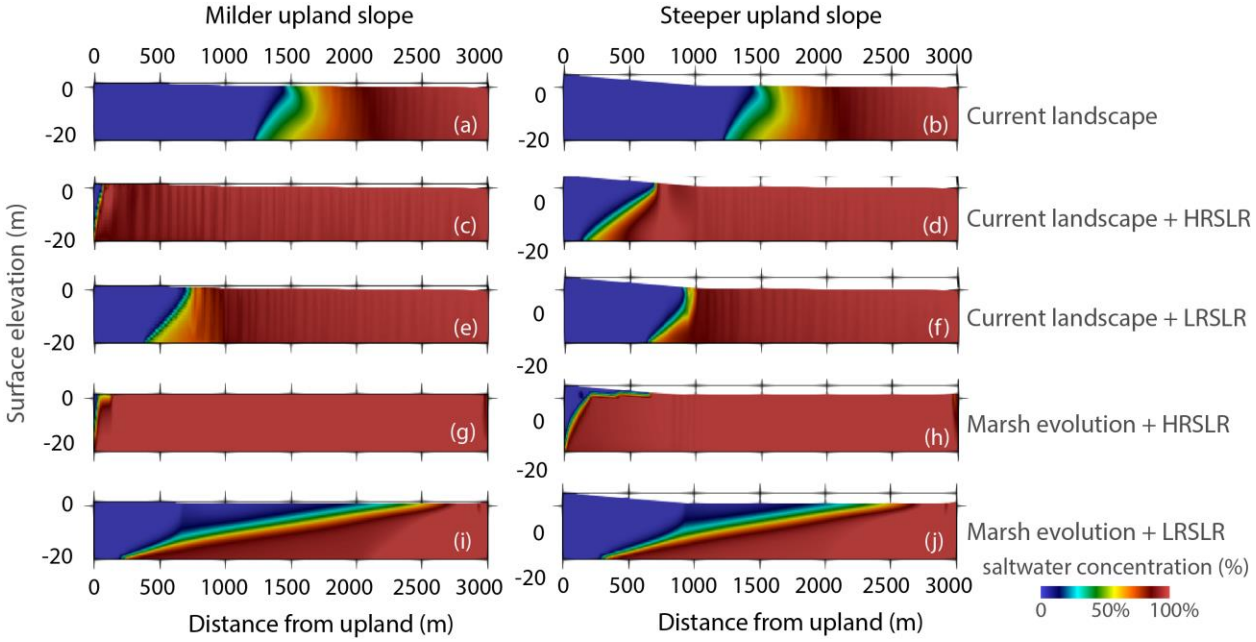

Figure 6. The distribution of subsurface saltwater concentration under the present-day sea level (a and b), future sea level (c,d, e, and f), and future sea level and topographic change (g, h, i, and j). All the simulation results are under the present-day upland GWT of 1.3 m. The left and right columns are the simulations with the milder and steeper upland slopes, respectively.

3.3 SWI under different upland GWT level

We also investigated the future SWI in response to the changes in upland GWT conditions caused by a wetter or drier future climate or intensified groundwater extraction (cases

5 to 12 in Table 2). With the same model settings and same SLR rate scenarios, a higher upland GWT (1.8 m above the initial MSL) under a wetter future climate causes a larger hydraulic gradient towards the ocean, thereby more freshwater flows towards the ocean. Therefore, the simulations predict a lower SWI for all cases under the high upland GWT (Fig. 7), compared with the cases under the present-day upland GWT (Fig. 6). Specifically, the cases without marsh evolution show slightly less SWI (Figs. 7c, d, e, and f), compared with the cases under the present-day GWT (Figs. 6c, d, e, and f). However, the cases with the marsh evolution and higher SLR rate show a larger decrease of SWI (Figs. 7g and h), compared with the corresponding cases under the present-day upland GWT (Figs. 6g and h). This is because the sufficient fresh groundwater supply from the upland pushes the saltwater back toward the ocean and dilutes the surface ponding saltwater.

However, with a lower upland GWT (0.9 m above the initial MSL) and under a drier future climate and/or increased groundwater extraction, the marshland creates a larger hydraulic gradient towards the land, compared with the present-day condition, causing more saltwater flows onto the marsh surface and into the aquifer. Therefore, more SWIs are observed in all simulation cases with the lower future upland GWT (Fig. 8). In particular, we see a larger increase of SWI for the cases with the marsh evolution and under the lower SLR rate (Figs. 8i and j), compared with the corresponding cases under the present-day upland GWT in Figs. 6i and j. This is because the upland groundwater supply is not sufficient to counteract the saltwater inflow.

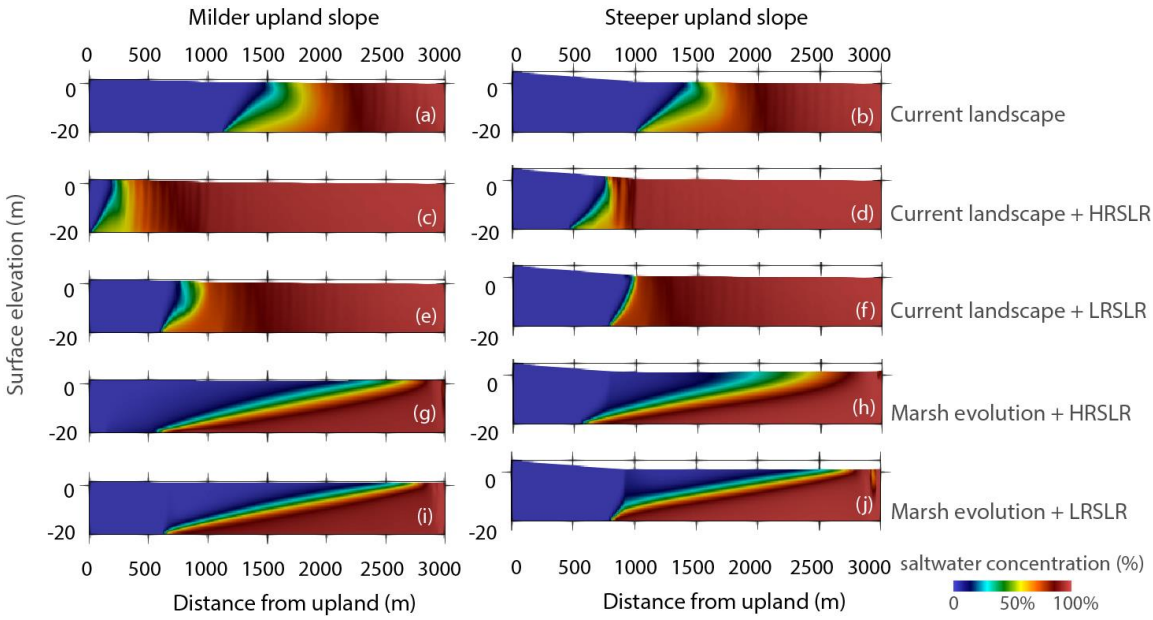

443
444 *Figure 7. The distribution of subsurface saltwater concentration under the present-day sea level (a and b), future sea level (c,d,*
445 *e, and f), and future sea level and topographic change (g, h, i, and j). All the simulation results are under the upland GWT of 1.8*
446 *m. The left and right columns are the simulations with the milder and steeper upland slopes, respectively.*

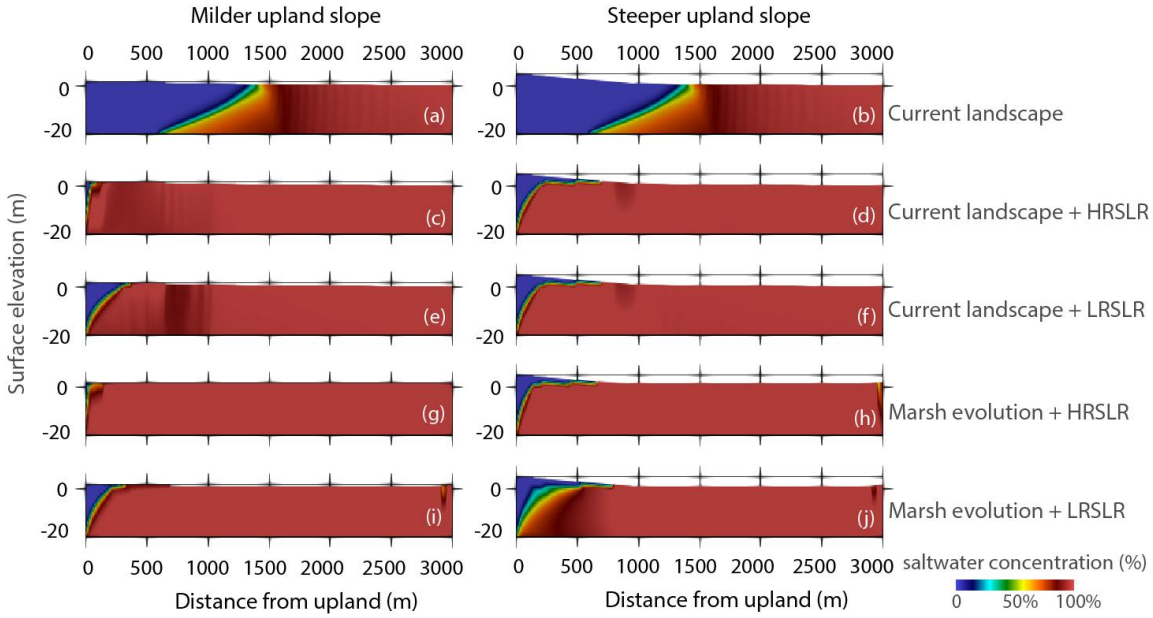

447
448
449 *Figure 8. The distribution of subsurface saltwater concentration under the present-day sea level (a and b), future sea level (c,d,*
450 *e, and f), and future sea level and topographic change (g, h, i, and j). All the simulation results are under the upland GWT of 0.9*
451 *m. The left and right columns are the simulations with the milder and steeper upland slopes, respectively.*

4 Discussion

4.1 Effect of coastal marsh evolution on coastal SWI

This study used a representative coastal marsh landscape to investigate the effect of coastal landscape evolution on coastal SWI under SLR. Our marsh evolution simulations confirmed that coastal marsh landscapes are dynamic, and the evolution of coastal marsh is very spatially heterogeneous in response to SLR (Fig. 2). We found that the future marsh topography has an important influence on coastal SWI, especially on the saltwater surface inflow, surface saltwater residence time, and saltwater infiltration. Firstly, the future evolved marsh topography significantly reduces the seawater inflow on the marsh surface because the increased marsh elevation near the ocean boundary reduces the hydraulic gradient between the marshland and the ocean (e.g., the saltwater inflows in Fig. 3). The predicted seawater inflow can be up to two orders of magnitude smaller than the inflow without considering marsh evolution implying that the seawater inflow may be overestimated in the studies that do not consider marsh evolution. Secondly, the depression zone formed during the marsh evolution processes can accumulate seawater, which significantly increases the saltwater residence time on the marsh surface and prolongs infiltration time. Therefore, with the evolved marsh landscape, the hydrologic regime may be very different from that without considering marsh evolution as we demonstrated above (e.g., Figs. 4, 5, 6, and S3). In addition, our numerical experiments show that the surface saltwater infiltration contributes more to the SWI than subsurface saltwater lateral inflow through ocean boundary. This finding is consistent with several previous studies, such as *Ataie-Ashtiani et al* (2013) who discussed the predominant effect of surface inundation on subsurface SWI.

4.2 The sensitivity of future SWI to upland groundwater supply

Our simulations under future SLR show that the upland GWT effect is more significant in the cases with marsh evolution because the exfiltrated freshwater can stay longer in the surface depression zone so that it has a larger influence on counteracting with surface saltwater inflow. For example, with the different upland GWTs, the cases with marsh evolution show larger variations in the displacements of the freshwater-saltwater interface (e.g., Figs 6, 7, and 8). Quantitatively, by compiling all the cases with the different upland GWTs in Figs. 6, 7, and 8, we found that the difference between the upland GWT and MHTL (GWT-MHTL) can be a good metric to understand the effect of marsh evolution on SWI under future SLR. Specifically, Figure 9 shows the mean distance between the freshwater-saltwater interface and the ocean boundary as a function of GWT-MHTL based on the cases in Figs. 6, 7, and 8. When GWT-MHTL is greater than zero (a hydraulic gradient towards the ocean), we found that the cases considering marsh evolution predict the shortest SWI distance (the orange dots and circles in Fig. 9). However, if GWT-MHTL is less than zero (a hydraulic gradient towards the inland), we observe a slight difference of SWI between the cases with and without marsh evolution. Therefore, as marshes evolve, the system may become more sensitive to the upland GWT variation, highlighting the importance of protecting upland groundwater resources to prevent intensified SWI in the future.

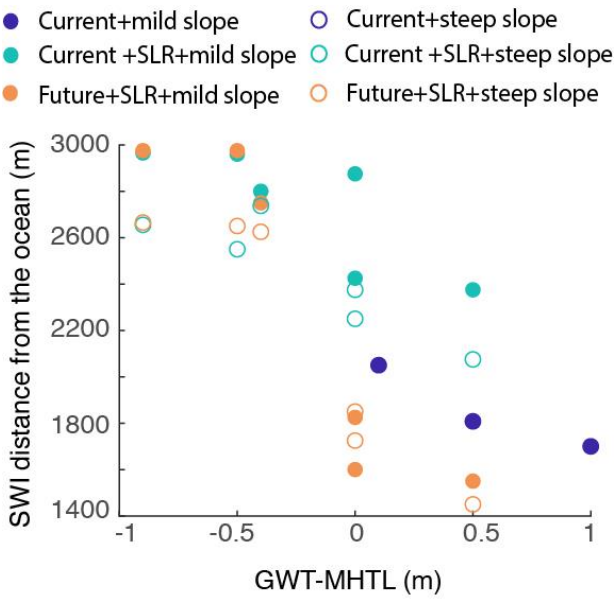

Figure 9. SWI distance as a function of GWT-MHTL under different SLR scenarios and upland slopes. The SWI distance was computed as the mean distance of the freshwater-saltwater interfaces from the ocean boundary. The terms, "current" and "future" in the legend, stand for current landscape topography and future marsh topography after marsh evolution. The circles and dots indicate the simulations under the milder and steeper upland slopes, respectively. Note: the blue circles and dots are overlapped when GWT-MHTL>0, so the blue circles are not visible.

4.3 Marsh evolution and its representativeness

Under the external drivers of SLR and tidal current, our marsh evolution simulations show that coastal marsh elevation is very likely to increase with a higher increase near the ocean boundary and a smaller increase landward due to a gradient in inorganic and organic sedimentations. Although the future marsh topographies predicted by our study are the results of the combined effect of the specific tidal amplitude, SLR rates, sediment concentration in the ocean, tidal period, and sediment diffusivity, the predicted topographic features (higher increase at ocean boundary and lower landward) are consistent with many previous marsh evolution studies (e.g., D'Alpaos et al., 2007; Kirwan, Walters, et al., 2016; Kirwan & Temmerman, 2009; Zhang et al., 2020). The formulations used in the Sed model to represent the dominant processes were selected from broadly-used sedimentation, erosion, and vegetation dynamic equations. The parameters used in this study were established in the literature from field measurements (Fagherazzi et al., 2013; Kirwan, Temmerman, et al., 2016; Morris et al., 2002; Mudd et al.,

2004) and were within the parameter range in the parametric sensitivity study by Zhang et al. (2020). Thus, our simulation results of marsh evolution are representative of the future marshland topographic change of some real-world coastal marshes under SLR.

4.4 The influence of future SWI on vegetation dynamics

Subsurface water salinity has a direct impact on vegetation growth, species richness, species distribution, and migration (Antonellini & Mollema, 2010; Silvestri & Marani, 2004). In previous studies that did not consider marsh evolution, the subsurface SWI was predicted to occupy a larger area of the coastal aquifers (e.g., Kuan et al., 2012; Michael et al., 2013), which exert larger stress on vegetation growth. However, our experiments show that the subsurface salinity may decrease, especially for the upper part of the aquifer, under the cases with a higher upland GWT and lower SLR rate (e.g., Figs. 6i and j and Figs. 7g, h, i, and j). Therefore, the surface ponding freshwater dilutes saltwater providing a favorable condition for salt-intolerant vegetation, which indicates that the vegetation species and distribution may be significantly different from the previous studies without considering marshland evolution.

4.5 Uncertainties and future work

In this study, we chose to focus on certain elements, including sea level, tide, upland groundwater table, and topographic change, which we felt were critical to our analysis of the coastal eco-geomorphologic impact on SWI. However, several factors may affect the SWI prediction, such as the vegetation dynamic representation, types of upland groundwater boundary condition, precipitation, evaporation, waves, and the land-river-ocean interaction. Specifically, our marsh evolution simulation assumed a linear relationship between the *Spartina*-dominant vegetation biomass and the coastal inundation level based on the field observation by *Morris et*

533 *al.* (2002). However, there are also other schemes to represent the relationship between
534 vegetation biomass and inundation level for different marsh landscapes, such as the *Spartina*-
535 nonlinear function (Mariotti & Fagherazzi, 2010) and mixed vegetation species linear function
536 (D'Alpaos et al., 2007). Zhang et al. (2020) evaluated the topographic outcomes from these three
537 vegetation schemes and found that all of the schemes predicted a higher elevation increase near
538 the ocean boundary and a lower increase landward. However, these schemes also showed
539 differences in marsh elevation relief and unvegetated-vegetated ratio. Therefore, it is worth
540 exploring SWI under future topographic change with different vegetation dynamic
541 representations. Our ongoing development of a physically-based vegetation dynamic
542 configuration on ATS will better link surface and subsurface water conditions, including salinity,
543 soil moisture, nutrient content, and inundation level, with vegetation growth. Therefore, the
544 newly developed model will better capture the vegetation dynamic features under different
545 subsurface salinity conditions, instead of only tracking the impact of surface inundation on
546 vegetation growth.

547 In addition, a constant GWT boundary condition is used in this study, which is suitable
548 for the coastal landscapes with a relatively small slope such as the slopes in our experiments
549 (Ketabchi et al., 2016). However, the freshwater supply from the upland can also be controlled
550 by continuous groundwater fluxes. Previous numerical and analytical modeling studies found
551 that SLR-induced saltwater intrusion has a larger impact on head-controlled coastal aquifers
552 rather than flux-controlled coastal aquifer (Rasmussen et al., 2013; Werner et al., 2012; Werner
553 & Simmons, 2009). Therefore, our study made a more aggressive prediction of SWI under SLR
554 based on the head-controlled systems. The SWI in a flux-controlled system will be explored in
555 future studies.

Precipitation and evaporation may also affect surface and subsurface saltwater transport and distribution (Geng et al., 2016; Payne, 2010; Werner & Simmons, 2009). To conduct this focused study, we reduced the complexity by limiting external drivers. We acknowledge that precipitation and evaporation would play an important role in changing water salinity on land surface and in the upper subsurface zone, yet they do not affect our conclusion on the role of marsh evolution in controlling the saltwater inflow and surface water residence time. However, to have a more realistic prediction of SWI for a real-world coastal marshland, it is necessary to take precipitation and evaporation into account in future studies.

Additionally, we did not consider erosion due to waves because marsh vegetation can mitigate waves if the waves are caused by the regular tidal variation and wind speed (D'Alpaos et al., 2007; Marani et al., 2007). However, under climatic extreme events, like hurricane and storm surge, the large waves may not be effectively mitigated by the marsh vegetation, and marshland erosion may occur and exceed the rate of sediment deposition. In this case, marsh elevation may decrease, especially near the ocean boundary as predicted by *Mariotti and Fagherazzi* (2010). The decrease of marsh elevation may increase surface saltwater inflow, thereby stimulating SWI. Also, hurricanes may directly cause distinct surface and subsurface water salinity distribution due to a dramatic increase in seawater level (Yu et al., 2016). Although it is not the scope of this study, it is worth exploring the effect of marsh evolution on SWI under these extreme climatic events in future studies.

Last, this study used transects that do not allow for surface water drainage paths connecting the marshland and marsh drainage network, which may facilitate the drainage of the surface ponding water to channels. This will require a 2-D simulation that captures the complex topography of marshes with channels and drainage pathways. Also, the role of 3-D

hydrodynamics is not considered and worthy of additional future study as it would incorporate baroclinic effects that can contribute to tidally-driven sedimentation.

5 Conclusions

In this study, we investigated the impact of coastal marsh evolution on SWI prediction under future SLR by using a physically-based coastal hydro-eco-geomorphologic model, ATS (Advanced Terrestrial Simulator). Using a representative coastal marsh landscape, we first predicted the marsh landscape change with different upland slopes and under two SLR scenarios. We found that the coastal marsh landscape is not static but dynamic in response to SLR. The marsh elevation increases with the rising sea level due to the organic and inorganic sedimentation and created a higher elevation near the ocean boundary and a depression zone in the middle of the marshland. The marsh accretion is projected to cause a significant reduction of saltwater inflow at the ocean boundary because of the decrease of the hydraulic gradient between the land and ocean. Also, the evolved topographic depression zone prolongs the residence time of surface ponding water, which affects surface saltwater infiltration, therefore causes distinct subsurface salinity distributions. With the evolved marsh landscape, we also tested the impact of different upland groundwater conditions on SWI under SLR, reflecting the impact of future drier/wetter climate conditions and human groundwater extraction on fresh groundwater dynamics. We found that with the topographic change in the future, SWI is more sensitive to the upland groundwater supply because of the more intensified freshwater-saltwater interaction in the depression zone. Therefore, when predicting future SWI on coastal marsh landscape, if we do not consider marsh evolution, we are very likely to overestimate SWI under future SLR if the upland GWT is higher than the MHTL, whereas we may underestimate SWI if the future upland GWT is lower than the MHTL.

602 This study highlighted the importance of considering coastal marsh landscape change in
603 predicting SWI under SLR, which was not investigated in previous studies. Over the decadal and
604 century scales, changes in coastal landscape topography can significantly affect the temporal and
605 spatial distributions of SWI under SLR. The insights gained from this study can help improve
606 our understanding of the vulnerability of coastal freshwater systems under SLR, marsh landscape
607 dynamics, and changes in upland groundwater resources, where these interconnections have been
608 previously ignored but warrant greater consideration.

609 **Acknowledgments**

610 The research presented in this paper was supported by the Laboratory Direct Research
611 and Development (LDRD) program at Los Alamos National Laboratory (LANL) under project
612 number 20180033DR. This study was also partially supported by the Center for Space and
613 Earth Sciences (CSES) Rapid Response Project at LANL under project number 20210528CR.
614 This research used resources provided by the Los Alamos National Laboratory Institutional
615 Computing Program, which is supported by the U.S. Department of Energy National Nuclear
616 Security Administration under Contract No. 89233218CNA000001.

617 This study is a model-based study that uses the ATS model and synthetic experiments.
618 The model source code is available in the model repositories from the Community Surface
619 Dynamics Modeling System (CSDMS)
620 https://csdms.colorado.edu/wiki/Model_download_portal. Model parameters are listed in the
621 tables above.

References

Antonellini, M., & Mollema, P. N. (2010). Impact of groundwater salinity on vegetation species richness in the coastal pine forests and wetlands of Ravenna, Italy. *Ecological Engineering*, *36*(9), 1201–1211. https://doi.org/10.1016/j.ecoleng.2009.12.007

Arcement, G. J., & Schneider, V. R. (1989). *Guide for selecting Manning's roughness coefficients for natural channels and flood plains* (USGS Numbered Series No. 2339). *Guide for selecting Manning's roughness coefficients for natural channels and flood plains* (Vol. 2339). U.S. G.P.O. ; For sale by the Books and Open-File Reports Section, U.S. Geological Survey,. https://doi.org/10.3133/wsp2339

Ataie-Ashtiani, B., Werner, A. D., Simmons, C. T., Morgan, L. K., & Lu, C. (2013). How important is the impact of land-surface inundation on seawater intrusion caused by sea-level rise? *Hydrogeology Journal*, *21*(7), 1673–1677. https://doi.org/10.1007/s10040-013-1021-0

Benson, C. H., Chiang, I., Chalermyanont, T., & Sawangsuriya, A. (2014). Estimating van Genuchten Parameters α and n for Clean Sands from Particle Size Distribution Data (pp. 410–427). Presented at the Soil Behavior Fundamentals to Innovations in Geotechnical Engineering, American Society of Civil Engineers. https://doi.org/10.1061/9780784413265.033

Best, Ü. S. N., Van der Wegen, M., Dijkstra, J., Willemsen, P. W. J. M., Borsje, B. W., & Roelvink, D. J. A. (2018). Do salt marshes survive sea level rise? Modelling wave action, morphodynamics and vegetation dynamics. *Environmental Modelling & Software*, *109*, 152–166. https://doi.org/10.1016/j.envsoft.2018.08.004

Burkett, V., & Kusler, J. (2000). CLIMATE CHANGE: POTENTIAL IMPACTS AND INTERACTIONS IN WETLANDS OF THE UNTTED STATES.

Carretero, S., Rapaglia, J., Bokuniewicz, H., & Kruse, E. (2013). Impact of sea-level rise on saltwater intrusion length into the coastal aquifer, Partido de La Costa, Argentina. *Continental Shelf Research*, *61–62*, 62–70. https://doi.org/10.1016/j.csr.2013.04.029

Chang, S. W., Clement, T. P., Simpson, M. J., & Lee, K.-K. (2011). Does sea-level rise have an impact on saltwater intrusion? *Advances in Water Resources*, *34*(10), 1283–1291. https://doi.org/10.1016/j.advwatres.2011.06.006

Chen, W.-B., Liu, W.-C., & Hsu, M.-H. (2015). Modeling assessment of a saltwater intrusion and a transport time scale response to sea-level rise in a tidal estuary. *Environmental Fluid Mechanics*, *15*(3), 491–514. https://doi.org/10.1007/s10652-014-9367-y

Coon, E. T., David Moulton, J., & Painter, S. L. (2016). Managing complexity in simulations of land surface and near-surface processes. *Environmental Modelling & Software*, *78*, 134–149. https://doi.org/10.1016/j.envsoft.2015.12.017

Da Lio, C., D'Alpaos, A., & Marani, M. (2013). The secret gardener: vegetation and the emergence of biogeomorphic patterns in tidal environments. *Philosophical Transactions of the Royal Society A: Mathematical, Physical and Engineering Sciences*, *371*(2004), 20120367.

D'Alpaos, A., Marani, M., & Rinaldo, A. (2007). Landscape evolution in tidal embayments: Modeling the interplay of erosion, sedimentation, and vegetation dynamics. *Journal of Geophysical Research: Earth Surface*, *112*(F1). https://doi.org/10.1029/2006JF000537

Fagherazzi, S., FitzGerald, D., Fulweiler, R., Hughes, Z., Wiberg, P., McGlathery, K., et al. (2013). Ecogeomorphology of salt marshes.

Fagherazzi, S., Anisfeld, S. C., Blum, L., Long, E. V., Feagin, R. A., Fernandes, A., et al. (2019). Sea Level Rise and the Dynamics of the Marsh-Upland Boundary. *Frontiers in Environmental Science*, *7*. https://doi.org/10.3389/fenvs.2019.00025

Ferguson, G., & Gleeson, T. (2012). Vulnerability of coastal aquifers to groundwater use and climate change. *Nature Climate Change*, *2*(5), 342–345. https://doi.org/10.1038/nclimate1413

Ganju, N. K., Defne, Z., & Fagherazzi, S. (2020). Are Elevation and Open-Water Conversion of Salt Marshes Connected? *Geophysical Research Letters*, *47*(3), e2019GL086703. https://doi.org/10.1029/2019GL086703

Geng, X., Boufadel, M. C., & Jackson, N. L. (2016). Evidence of salt accumulation in beach intertidal zone due to evaporation. *Scientific Reports*, *6*(1), 31486. https://doi.org/10.1038/srep31486

Giambastiani, B. M. S., Antonellini, M., Oude Essink, G., & Stuurman, R. (2007). Saltwater intrusion in the unconfined coastal aquifer of Ravenna (Italy): A numerical model. *Journal of Hydrology*, *340*(1–2), 91–104. https://doi.org/10.1016/j.jhydrol.2007.04.001

Guimond, J., & Tamborski, J. (2021). Salt Marsh Hydrogeology: A Review. *Water*, *13*(4), 543. https://doi.org/10.3390/w13040543

676 Herbert, A. W., Jackson, C. P., & Lever, D. A. (1988). Coupled groundwater flow and solute transport with fluid
677 density strongly dependent upon concentration. *Water Resources Research*, *24*(10), 1781–1795.
678 https://doi.org/10.1029/WR024i010p01781
679 Hughes, J. D., Vacher, H. L., & Sanford, W. E. (2009). Temporal response of hydraulic head, temperature, and
680 chloride concentrations to sea-level changes, Floridan aquifer system, USA. *Hydrogeology Journal*, *17*(4),
681 793–815. https://doi.org/10.1007/s10040-008-0412-0
682 Ketabchi, H., Mahmoodzadeh, D., Ataie-Ashtiani, B., Werner, A. D., & Simmons, C. T. (2014). Sea-level rise
683 impact on fresh groundwater lenses in two-layer small islands. *Hydrological Processes*, *28*(24), 5938–
684 5953. https://doi.org/10.1002/hyp.10059
685 Ketabchi, H., Mahmoodzadeh, D., Ataie-Ashtiani, B., & Simmons, C. T. (2016). Sea-level rise impacts on seawater
686 intrusion in coastal aquifers: Review and integration. *Journal of Hydrology*, *535*, 235–255.
687 https://doi.org/10.1016/j.jhydrol.2016.01.083
688 Kirwan, M., & Murray, A. B. (2007). A coupled geomorphic and ecological model of tidal marsh evolution.
689 *Proceedings of the National Academy of Sciences*, *104*(15), 6118–6122.
690 https://doi.org/10.1073/pnas.0700958104
691 Kirwan, M., & Temmerman, S. (2009). Coastal marsh response to historical and future sea-level acceleration.
692 *Quaternary Science Reviews*, *28*(17), 1801–1808. https://doi.org/10.1016/j.quascirev.2009.02.022
693 Kirwan, M., Temmerman, S., Skeehan, E. E., Guntenspergen, G. R., & Fagherazzi, S. (2016). Overestimation of
694 marsh vulnerability to sea level rise. *Nature Climate Change*, *6*(3), 253–260.
695 https://doi.org/10.1038/nclimate2909
696 Kirwan, M., Walters, D. C., Reay, W. G., & Carr, J. A. (2016). Sea level driven marsh expansion in a coupled model
697 of marsh erosion and migration. *Geophysical Research Letters*, *43*(9), 4366–4373.
698 https://doi.org/10.1002/2016GL068507
699 Kuan, W. K., Jin, G., Xin, P., Robinson, C., Gibbes, B., & Li, L. (2012). Tidal influence on seawater intrusion in
700 unconfined coastal aquifers. *Water Resources Research*, *48*(2). https://doi.org/10.1029/2011WR010678
701 Kuan, W. K., Xin, P., Jin, G., Robinson, C. E., Gibbes, B., & Li, L. (2019). Combined Effect of Tides and Varying
702 Inland Groundwater Input on Flow and Salinity Distribution in Unconfined Coastal Aquifers. *Water*
703 *Resources Research*, *55*(11), 8864–8880. https://doi.org/10.1029/2018WR024492

704 Langevin, C. D., & Zygnerski, M. (2013). Effect of Sea-Level Rise on Salt Water Intrusion near a Coastal Well
705 Field in Southeastern Florida. *Groundwater*, *51*(5), 781–803. https://doi.org/10.1111/j.1745-
706 6584.2012.01008.x
707 Loáiciga, H. A., Pingel, T. J., & Garcia, E. S. (2012). Sea Water Intrusion by Sea-Level Rise: Scenarios for the 21st
708 Century. *Groundwater*, *50*(1), 37–47. https://doi.org/10.1111/j.1745-6584.2011.00800.x
709 Lu, C., Xin, P., Li, L., & Luo, J. (2015). Seawater intrusion in response to sea-level rise in a coastal aquifer with a
710 general-head inland boundary. *Journal of Hydrology*, *522*, 135–140.
711 https://doi.org/10.1016/j.jhydrol.2014.12.053
712 Marani, M., D'Alpaos, A., Lanzoni, S., Carniello, L., & Rinaldo, A. (2007). Biologically-controlled multiple
713 equilibria of tidal landforms and the fate of the Venice lagoon. *Geophysical Research Letters*, *34*(11).
714 Mariotti, G., & Fagherazzi, S. (2010). A numerical model for the coupled long-term evolution of salt marshes and
715 tidal flats. *Journal of Geophysical Research: Earth Surface*, *115*(F1).
716 https://doi.org/10.1029/2009JF001326
717 Masterson, J. P., & Garabedian, S. P. (2007). Effects of Sea-Level Rise on Ground Water Flow in a Coastal Aquifer
718 System. *Groundwater*, *45*(2), 209–217. https://doi.org/10.1111/j.1745-6584.2006.00279.x
719 Mazi, K., Koussis, A. D., & Destouni, G. (2013). Tipping points for seawater intrusion in coastal aquifers under
720 rising sea level. *Environmental Research Letters*, *8*(1), 014001. https://doi.org/10.1088/1748-
721 9326/8/1/014001
722 Michael, H. A., Russoniello, C. J., & Byron, L. A. (2013). Global assessment of vulnerability to sea-level rise in
723 topography-limited and recharge-limited coastal groundwater systems. *Water Resources Research*, *49*(4),
724 2228–2240.
725 Morgan, L. K., Stoeckl, L., Werner, A. D., & Post, V. E. A. (2013). An assessment of seawater intrusion overshoot
726 using physical and numerical modeling. *Water Resources Research*, *49*(10), 6522–6526.
727 https://doi.org/10.1002/wrcr.20526
728 Morris, J. T., Sundareshwar, P., Nietch, C. T., Kjerfve, B., & Cahoon, D. R. (2002). Responses of coastal wetlands
729 to rising sea level. *Ecology*, *83*(10), 2869–2877.

730 Morris, J. T., Barber, D. C., Callaway, J. C., Chambers, R., Hagen, S. C., Hopkinson, C. S., et al. (2016).
731 Contributions of organic and inorganic matter to sediment volume and accretion in tidal wetlands at steady
732 state. *Earth's Future*, *4*(4), 110–121. https://doi.org/10.1002/2015EF000334
733 Mudd, S. M., Fagherazzi, S., Morris, J. T., & Furbish, D. J. (2004). Flow, sedimentation, and biomass production on
734 a vegetated salt marsh in South Carolina: toward a predictive model of marsh morphologic and ecologic
735 evolution. *The Ecogeomorphology of Tidal Marshes, Coastal Estuarine Stud*, *59*, 165–187.
736 Oude Essink, G., Van Baaren, E. S., & De Louw, P. G. (2010). Effects of climate change on coastal groundwater
737 systems: A modeling study in the Netherlands. *Water Resources Research*, *46*(10).
738 Parchure Trimbak M. & Mehta Ashish J. (1985). Erosion of Soft Cohesive Sediment Deposits. *Journal of Hydraulic*
739 *Engineering*, *111*(10), 1308–1326. https://doi.org/10.1061/(ASCE)0733-9429(1985)111:10(1308)
740 Payne, D. F. (2010). Effects of Sea-Level Rise and Pumpage Elimination on Saltwater Intrusion in the Hilton Head
741 Island Area, South Carolina, 2004—2104. *U.S. Geological Survey Scientific Investigations Report 2009–*
742 *5251*, 83.
743 Rasmussen, P., Sonnenborg, T. O., Goncear, G., & Hinsby, K. (2013). Assessing impacts of climate change, sea
744 level rise, and drainage canals on saltwater intrusion to coastal aquifer. *Hydrology and Earth System*
745 *Sciences*, *17*(1), 421–443. https://doi.org/10.5194/hess-17-421-2013
746 Riazi, A., & Türker, U. (2019). The drag coefficient and settling velocity of natural sediment particles.
747 *Computational Particle Mechanics*, *6*(3), 427–437. https://doi.org/10.1007/s40571-019-00223-6
748 Richards, L. A. (1931). Capillary conduction of liquids through porous mediums. *Physics*, *1*(5), 318–333.
749 https://doi.org/10.1063/1.1745010
750 Sanford, W. E., Pope, J. P., Selnick, D. L., & Stumvoll, R. F. (2012). *Simulation of Groundwater Flow in the*
751 *Shallow Aquifer System of the Delmarva Peninsula, Maryland and Delaware* (U.S. Geological Survey
752 Open-File Report No. 2012–1140) (p. 58). USGS. Retrieved from https://pubs.usgs.gov/of/2012/1140/
753 Sefelnasr, A., & Sherif, M. (2014). Impacts of Seawater Rise on Seawater Intrusion in the Nile Delta Aquifer,
754 Egypt. *Groundwater*, *52*(2), 264–276. https://doi.org/10.1111/gwat.12058
755 Silvestri, S., & Marani, M. (2004). Salt-marsh vegetation and morphology: Basic physiology, modelling and remote
756 sensing observations. *The Ecogeomorphology of Tidal Marshes, Coastal Estuarine Stud*, *59*, 5–25.

Simmons, C. T., Fenstemaker, T. R., & Sharp, J. M. (2001). Variable-density groundwater flow and solute transport in heterogeneous porous media: approaches, resolutions and future challenges. *Journal of Contaminant Hydrology*, *52*(1), 245–275. https://doi.org/10.1016/S0169-7722(01)00160-7

Sorensen, R. M., Weisman, R. N., & Lennon, G. P. (1984). Control of Erosion, Inundation, and Salinity Intrusion Caused by Sea Level Rise. In M. C. Barth & J. G. Titus (Eds.), *Greenhouse Effect and Sea Level Rise* (pp. 179–214). Boston, MA: Springer US. https://doi.org/10.1007/978-1-4684-6569-3_6

Sousa, A. I., Lillebø, A. I., Pardal, M. A., & Caçador, I. (2010). Productivity and nutrient cycling in salt marshes: contribution to ecosystem health. *Estuarine, Coastal and Shelf Science*, *87*(4), 640–646.

Spencer, T., Schuerch, M., Nicholls, R. J., Hinkel, J., Lincke, D., Vafeidis, A. T., et al. (2016). Global coastal wetland change under sea-level rise and related stresses: The DIVA Wetland Change Model. *Global and Planetary Change*, *139*, 15–30. https://doi.org/10.1016/j.gloplacha.2015.12.018

Thompson, C. E. L., Amos, C. L., & Umgiesser, G. (2004). A comparison between fluid shear stress reduction by halophytic plants in Venice Lagoon, Italy and Rustico Bay, Canada—analyses of in situ measurements. *Journal of Marine Systems*, *51*(1), 293–308. https://doi.org/10.1016/j.jmarsys.2004.05.017

Tiner, R. W. (2013). *Tidal Wetlands Primer*. University of Massachusetts Press.

Vandenbohede, A., Luyten, K., & Lebbe, L. (2008). Effects of Global Change on Heterogeneous Coastal Aquifers: A Case Study in Belgium. *Journal of Coastal Research*, *24*(sp2), 160–170. https://doi.org/10.2112/05-0447.1

Vreugdenhil, C. B. (1994). Shallow-water flows. In C. B. Vreugdenhil (Ed.), *Numerical Methods for Shallow-Water Flow* (pp. 1–14). Dordrecht: Springer Netherlands. https://doi.org/10.1007/978-94-015-8354-1_1

Vu, D. T., Yamada, T., & Ishidaira, H. (2018). Assessing the impact of sea level rise due to climate change on seawater intrusion in Mekong Delta, Vietnam. *Water Science and Technology*, *77*(6), 1632–1639. https://doi.org/10.2166/wst.2018.038

Watson, T. A., Werner, A. D., & Simmons, C. T. (2010). Transience of seawater intrusion in response to sea level rise. *Water Resources Research*, *46*(12). https://doi.org/10.1029/2010WR009564

Werner, A. D., & Simmons, C. T. (2009). Impact of Sea-Level Rise on Sea Water Intrusion in Coastal Aquifers. *Groundwater*, *47*(2), 197–204. https://doi.org/10.1111/j.1745-6584.2008.00535.x

784 Werner, A. D., Ward, J. D., Morgan, L. K., Simmons, C. T., Robinson, N. I., & Teubner, M. D. (2012).
785 Vulnerability Indicators of Sea Water Intrusion. *Groundwater*, *50*(1), 48–58.
786 https://doi.org/10.1111/j.1745-6584.2011.00817.x
787 Winn, K. O., Saynor, M. J., Eliot, M. J., & Elio, I. (2006). Saltwater Intrusion and Morphological Change at the
788 Mouth of the East Alligator River, Northern Territory. *Journal of Coastal Research*, *2006*(221), 137–149.
789 https://doi.org/10.2112/05A-0011.1
790 Yang, J., Graf, T., & Ptak, T. (2015). Sea level rise and storm surge effects in a coastal heterogeneous aquifer: a 2D
791 modelling study in northern Germany. *Grundwasser*, *20*(1), 39–51. https://doi.org/10.1007/s00767-014-
792 0279-z
793 Yu, X., Yang, J., Graf, T., Koneshloo, M., O'Neal, M. A., & Michael, H. A. (2016). Impact of topography on
794 groundwater salinization due to ocean surge inundation. *Water Resources Research*, *52*(8), 5794–5812.
795 https://doi.org/10.1002/2016WR018814
796 Zhang, Y., Li, W., Sun, G., Miao, G., Noormets, A., Emanuel, R., & King, J. S. (2018). Understanding coastal
797 wetland hydrology with a new regional-scale, process-based hydrological model. *Hydrological Processes*,
798 *32*(20), 3158–3173. https://doi.org/10.1002/hyp.13247
799 Zhang, Y., Li, W., Sun, G., & King, J. S. (2019). Coastal wetland resilience to climate variability: A hydrologic
800 perspective. *Journal of Hydrology*, *568*, 275–284. https://doi.org/10.1016/j.jhydrol.2018.10.048
801 Zhang, Y., Rowland, J. C., Xu, C., Wolfram, P. J., Svyatsky, D., Moulton, J. D., et al. (2020). Understanding the
802 Eco-Geomorphologic Feedback of Coastal Marsh Under Sea Level Rise: Vegetation Dynamic
803 Representations, Processes Interaction, and Parametric Sensitivity. *Journal of Geophysical Research: Earth*
804 *Surface*, *125*(11), e2020JF005729. https://doi.org/10.1029/2020JF005729
805